PHYSICAL REVIEW B **82**, 144113 (2010)

Strained state dynamics in a VO_2 thin film

T. Kikuzuki, R. Takahashi, and M. Lippmaa*
Institute for Solid State Physics, University of Tokyo, Chiba 277-8581, Japan
(Received 17 May 2010; revised manuscript received 27 September 2010; published 20 October 2010)

The dynamics of a strain-induced resistive phase transition in a VO_2 thin film was studied by using a low-frequency crystal bending stage. It was found that the resistance response of the film to strain excitation is determined by two time constants, interpreted as a nucleation lifetime, in the 10^{-6}–10^{-4} s range, and a domain growth lifetime of $\sim 10^{-3}$ s. The variation of the domain nucleation lifetime is discussed in terms of the barrier height separating the coexisting insulating and metallic phases in a VO_2 film. Below the transition temperature, the phase transition is nucleation limited. Above the transition temperature, the resistance change is strongly affected by the growth of metallic domains. Direct imaging of metallic domains by local-probe current mapping showed that the phase transition in a thin film is limited by the presence of grain boundaries.

DOI: 10.1103/PhysRevB.82.144113 PACS number(s): 71.30.+h, 68.35.Rh, 64.70.Nd

I. INTRODUCTION

The first-order metal-insulator transition that occurs in nondoped VO_2 at around 340 K was originally reported by Morin[1] and has been the subject of active research ever since.[2] The transition temperature is high enough for various room-temperature sensor applications, such as uncooled microbolometer infrared cameras.[3] The resistive transition in VO_2 is accompanied by a structural change from a metallic high-temperature tetragonal (rutile-$P4_2/mnm$) phase to a low-temperature semiconducting monoclinic ($P2_1/c$) phase. As has been pointed out by Goodenough,[4] the structural transition consists of two distinct features: a dimerization of the vanadium bonds along the c axis of the tetragonal phase and an antiferroelectric distortion of the oxygen octahedra surrounding the vanadium atoms. Due to this, the metal-insulator transition in VO_2 is usually referred to as a simultaneous Mott-Peierls transition and a question arises as to what drives the temperature-dependent phase transition, an electronic Mott mechanism or thermal structural change, which leads to a Peierls transition.[2]

The nature of the metallic and insulating phases can be studied in steady state as a function of temperature by, for example, optical conductivity measurements.[5] In order to distinguish electronic effects from structural changes, it is possible to separate different stages of the transition in time. This has been done by inducing additional carriers by femtosecond light pulses and observing the response of the crystal by terahertz (THz) spectroscopy[6,7] or electron diffraction.[8] While the electronic transition has been shown to be a subpicosecond process, and thus much faster than the lattice response, intense optical pumping is always accompanied by heating, and it can thus be difficult to distinguish between electronically and thermally induced lattice changes. For observing slower, electronically induced phase transitions, application of an electric field to a VO_2 thin film has been used, although for direct current injection, heating still affects the measurements.[9] Carrier injection in heterostructures under high electric fields has been used to avoid heating.[10]

In this work, we study the dynamics of the phase transition in VO_2 thin films under reversible strain conditions.[11] Application of uniaxial strain to a thin-film sample offers a unique possibility of changing only the lattice degrees of freedom without changing the carrier density and without affecting the temperature. In this case, strain is applied by bending the substrate on which a thin VO_2 film has been grown. While most strain effect studies focus either on large static pressure of up to about 100 GPa for diamond anvil cells or small stress at very high frequencies, as in piezoelectric bulk materials ($\sim$10 kHz and $\sim$10 kPa), the technique used in this work allows us to probe relatively large strains of up to about 0.05% in the plane of the film at frequencies of up to 1 kHz. This strain scale is comparable to what can be achieved with piezoelectric substrates[12] and is sufficient to affect the phase balance between the insulating and metallic domains in a mixed-state film close to the transition temperature. The time scales that we probe are suitable for studying domain switching dynamics.

II. EXPERIMENT

The VO_2 films used for strain measurements were grown on $9\times3\times0.2$ mm^3 nondoped $TiO_2(001)$ substrates by pulsed laser deposition. A polycrystalline V_2O_3 target was used for ablation at a laser fluence of 0.6 J/cm^2 and a background oxygen pressure of 4.4 mTorr. The ablation laser (KrF, $\lambda=248$ nm) operated at 1 Hz. The film used in this study had a thickness of 12.5 nm and was grown at a substrate temperature of 480 °C.

The most important factors that can affect the stoichiometry and microstructure of a VO_2 thin film are the deposition rate and the background oxygen pressure. In order to obtain the correct VO_2 phase, the oxygen pressure had to be set with an accuracy of 0.1 mTorr while the slowest practical growth rate of 0.05 Å/pulse gave the largest resistance change at the phase transition temperature. These two growth parameters are related and the strong effect of the growth rate on film stoichiometry points to the slow oxidation kinetics of the film during the relatively low-temperature growth. The surface morphology and grain structure were studied by noncontact atomic force microscopy (AFM).

Similar VO_2 films were grown on metallic Nb-doped $TiO_2(001)$ substrates at the same deposition conditions for

 ©2010 The American Physical Society

observing temperature-dependent domain morphologies by conducting-tip AFM (CT-AFM). The purpose was to correlate the observed strain relaxation in films under dynamic strain with the temperature-dependent domain-switching dynamics. The shape and size of metallic domains in the films were detected by measuring current maps by CT-AFM while the sample temperature was changed by a heater element embedded in the sample holder. The resistance behavior measured by attaching electrodes to the film surface by silver paste bonding was very similar to the films grown on insulating $TiO_2(001)$ substrates.

For films grown on nondoped substrates, transport measurements were performed by evaporating aluminum electrodes on the film surface and wire bonding aluminum lead wires by ultrasonic bonding to the aluminum electrode pads. Resistance measurements were performed in a two-point geometry over an electrode gap of 0.2 mm. The absolute resistance values thus have some uncertainty due to the contact resistance contribution but this does not affect the time dependence of resistance in dynamic strain measurements. The presence of the resistive transition in the film was verified in a separate measurement in a four-point geometry as well.

Dynamic strain measurements were performed by mounting a VO_2 thin film sample in a temperature-controlled crystal bending stage.[11] This system allowed the substrate crystal to be deformed in a three-point geometry by applying pressure in the center of the crystal with a piezoelectric actuator while the edges of the substrate were fixed to the bending stage frame. Pressure from the actuator deformed the planar sample, consisting of a 12.5-nm-thick film on a 200-μm-thick substrate, into a cylindrical shape, applying uniaxial in-plane tensile strain on the film. The actual sample surface deformation while bending the crystal was measured with a Hartmann-type wavefront analyzer.[13] The change of the in-plane lattice parameter, δ_{ab}, was calculated from the measured surface deformation. The corresponding compressive change in the out-of-plane lattice parameter, δ_c, was calculated from the Poisson ratio of VO_2.[14] The maximum in-plane strain that could be applied to a 0.2 mm TiO_2 substrate in this way was limited by the cracking of the substrate crystal to $\delta_{ab} \sim 0.05\%$, which corresponds to a maximum out-of-plane strain of $\delta_c = 0.02\%$. The out-of-plane c-axis direction in this case corresponds to the dimerization axis of vanadium bonds in the monoclinic insulating phase of the film. The sample temperature was controlled in the range of 295–315 K by attaching a miniature thermistor to the film surface and using a feedback system to adjust the current through a Si heater element at the back of the substrate.

III. RESULTS AND DISCUSSION

The crystallinity, strain, and orientation of the films were checked by conventional symmetric Cu $K\alpha$ x-ray diffraction (XRD). As shown in the diffraction pattern in Fig. 1, the film was c-axis oriented and nearly fully strained. The in-plane lattice mismatch between a $TiO_2(001)$ substrate and bulk c-axis-oriented VO_2 is 0.86%. An epitaxial VO_2 film is thus under tensile in-plane strain and compressive out-of-plane c-axis strain. The film peak spread in the XRD pattern shows

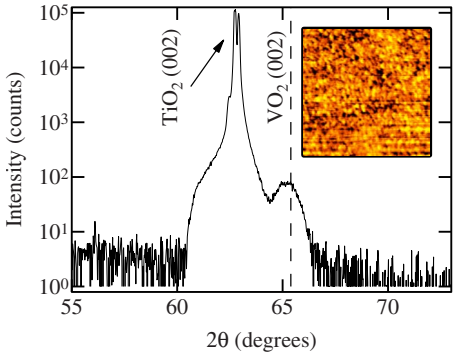

FIG. 1. (Color online) X-ray diffraction pattern of a strained VO_2 film on a $TiO_2(001)$ substrate. The vertical dashed line marks the expected film peak position for a fully-strained epitaxial film. Inset shows a 0.5 μm^2 AFM topography image of the film surface. Measurements were done at room temperature with the film in the insulating state with a monoclinic structure.

that there is some strain relaxation in the film. An AFM image of a film grown on a Nb-doped TiO_2 substrate is shown in the inset. The grain structure evident in the image is probably the result of partial in-plane strain relaxation. The average grain diameter was 21 nm and did not correlate strongly with the flatness of the original substrate surface. On a microscopic scale, partial strain relaxation would result in different grains possessing slightly different transition temperatures, T_c. It is known from strain studies that the T_c of epitaxial VO_2 films is a function of the c-axis strain with a proportionality factor in the range of 30–50 K/%.[11,15] For films grown on $TiO_2(001)$ substrates, the film is compressively strained along the out-of-plane c-axis direction. Due to this, T_c can be suppressed from the bulk value of 340 K to temperatures as low as 290 K.[15] For partially strained films, intermediate values can be seen, depending on the growth parameters. For the film studied in this work, the transition temperature was 308 K with a hysteresis width of 0.7 K (Fig. 2). The level of strain relaxation is largely determined by the growth temperature with lower growth temperatures generally leading to larger strain in the film. Changes in the grain size, which is affected not only by growth parameters, but

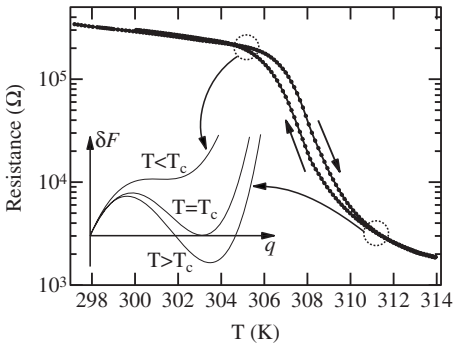

FIG. 2. Resistance vs temperature of a VO_2 thin film grown on a $TiO_2(001)$ substrate. Free-energy profiles calculated by Vikhnin *et al.* (Ref. 16) are shown in terms of the charge-transfer order parameter, q for the tetragonal symmetry, i.e., q is bigger in the metallic phase, which is energetically favored when $T > T_c$.

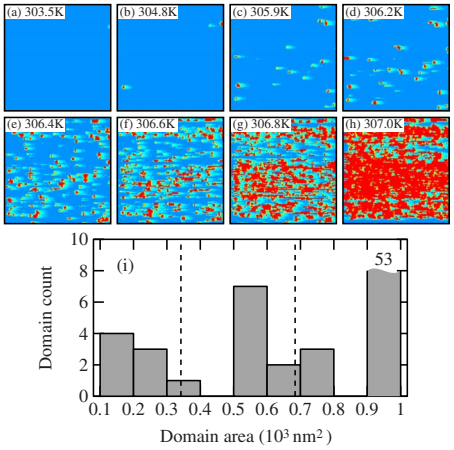

FIG. 3. (Color online) [(a)–(h)] Conducting-tip AFM current map images covering a 1×1 μm^2 area, measured during cooling of a VO_2 film sample from 307 to 303.5 K. The measurement temperature for each map is shown in the image label. The mapping was done at a tip bias of −1 V. Light (blue) regions correspond to insulating domains and dark (red) dots show the appearance of the metallic state. The light blue tails surrounding metallic domains are caused by the limited bandwidth of the AFM tip current detector but correspond to tip currents that are below the threshold used for domain size determination. (i) A histogram of metallic domain sizes measured from images (a)–(d). Vertical dashed lines mark integer multiples of the average grain size of 342 nm^2, determined from the topography image. Based on the minimum detectable feature size, the image resolution is limited by the 128 pixel square imaging raster.

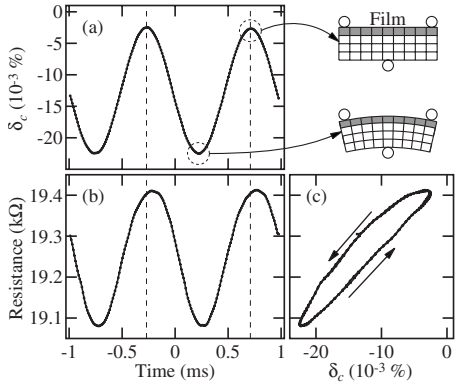

FIG. 4. (a) Compressive *c*-axis strain applied to a film by flexing the substrate at 1 kHz and (b) the corresponding film resistance change. Schematic views of the deformation states are also shown (Ref. 11). (c) Resistance response hysteresis under harmonic strain excitation, replotted from (a) and (b).

also by the quality of the starting substrate surface, mostly affect the width of the hysteresis and the temperature coefficient of resistance at T_c.

It is known that in VO_2 thin films close to the transition temperature, both metallic and insulating phases can coexist. The balance between the metallic and insulating domains in a film sample can obviously be changed by temperature[3,17] but also by light excitation,[16] electric field,[9,10] epitaxial strain,[15,18] and perhaps even magnetic field.[19] Infrared[17] and THz spectroscopy[20] measurements have shown that the evolution of the metallic phase during heating proceeds through domain nucleation and growth, rather than a homogeneous phase change. Direct imaging by local-probe light scattering[21,22] has been used to visualize the formation of submicron metallic domains as a function of temperature. In thin films, the spatial distribution of metallic and insulating domains can presumably be affected by the presence of crystal grains,[23] as has been suggested based on scanning tunneling spectroscopy mapping experiments.[24] The dynamics of the transition in thin film samples can also be affected by the presence of defects and oxygen nonstoichiometry.[25]

In order to determine the effect of crystal grains on the phase transition dynamics, CT-AFM images of a VO_2 film on a metallic $Nb:TiO_2$ substrate were measured during cooling through the phase transition temperature. The current map images are shown in Fig. 3. The insulating domains (blue, light) dominate the system at low temperature while metallic domains (red, dark) dominate at high temperature. The area for each domain type can be calculated by standard image particle analysis. A histogram of domain sizes, calculated for small isolated domains in Figs. 3(a)–3(d), is shown in Fig. 3(i). It is clear that the metallic domain sizes cluster at values that are approximate multiples of the average grain size determined from the topography image shown in the Fig. 1 inset. This behavior is consistent with domain growth that occurs by switching individual crystal grains between the metallic and insulating states. The data does not indicate the occurrence of partial grain switching as has been observed for less strained films grown by the sol-gel method on sapphire.[22] As the temperature of a VO_2 film is increased, a conducting path forms in the film by metallic domain growth until finally a percolative threshold is reached.

On a single grain level, the phase transition is limited by the ability to nucleate a metallic (or insulating) grain-wide phase transition, upon which the *c*-axis length of a grain changes by up to about 0.5%. If strain coupling exists between grains, the nucleation probability for a grain may depend on whether the grain is on a metallic domain boundary or not. This effect is difficult to determine from the AFM data alone, but can be addressed by looking at a dynamic strain response of the film.

Dynamic strain measurements were performed at a fixed temperature close to the phase transition point. The effect of *c*-axis strain, applied in a temperature range where metallic and insulating phases can coexist, is to reversibly switch a small population of grains in the film, resulting in a small but easily detectable resistance change.

A typical dynamic strain measurement result, where the strain-induced resistance change was measured at a fixed temperature near T_c, is shown in Fig. 4. Dynamic strain measurements were done at frequencies of up to 1 kHz. A small hysteresis for a harmonic strain input was observed, as shown in Fig. 4(c). The behavior is qualitatively similar to the hysteresis behavior seen in the temperature scan in Fig. 2.

In the following analysis, we mostly look at the relative resistance change, or a resistance response ratio, defined as $\Delta R_{\text{strain}}(t)/R_0(\%)$, where $\Delta R_{\text{strain}}(t)$ is the time-dependent resistance change induced by dynamic strain and R_0 is the

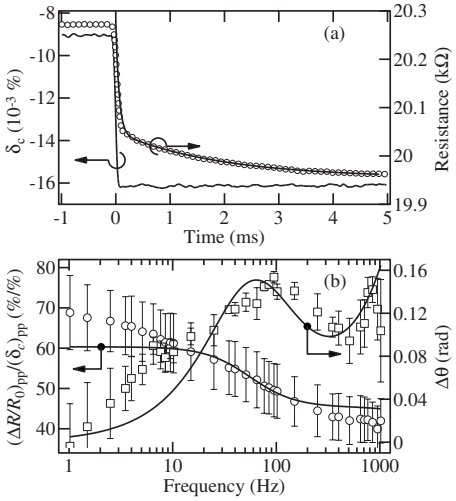

FIG. 5. (a) Fitting the time dependence of resistance after a stepwise strain excitation at T_c with Eq. (1) suggests a double exponential response function. (b) Frequency dependence of strain response amplitude (circles) and phase shift (squares) at T_c, together with fitting curves.

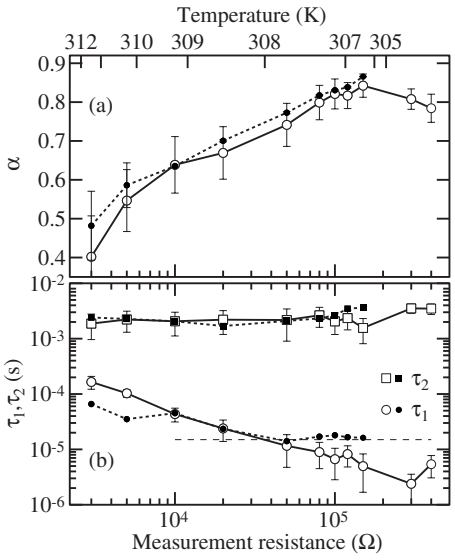

FIG. 6. Measurement resistance (temperature) dependence of the (a) α and (b) τ_1, and τ_2 parameters. Open markers correspond to values obtained from frequency-domain measurements as shown in Fig. 5(b). Filled markers and dotted lines correspond to time-domain data as shown in Fig. 5(a). The horizontal dashed line in (b) marks the time resolution limit of the time-domain measurement of τ_1.

maximum resistance. This particular scaling is used because the crystal bending stage can only apply an unsymmetric compressive out-of-plane strain on the sample. In this experiment, strain thus always reduces the sample resistance relative to the unstrained equilibrium value R_0. A phase delay between the harmonic strain input and the resistance response is defined as $\Delta\phi$ (rad).

A common feature of all dynamic strain measurements (Fig. 4) was an increase of the phase delay, $\Delta\phi$, and a drop of resistance change amplitude, ΔR_{strain}, with increasing frequency. This behavior is characteristic of a damped oscillator where the particular relaxation mechanism responsible for the damping can be deduced by measuring either a time or frequency response of the system. The measured time dependence of resistance after a stepwise strain change shown in Fig. 5(a) suggests that an appropriate model for $\Delta R_{\text{strain}}(t)/R_0$ would be a double exponential function

$$\frac{\Delta R_{\text{strain}}(t)}{R_0} \propto 1 - \alpha \exp\left(-\frac{t}{\tau_1}\right) - (1-\alpha)\exp\left(-\frac{t}{\tau_2}\right), \quad (1)$$

where t is time, τ_1 and $\tau_2(\tau_2 > \tau_1)$ are time constants, and α is a scaling factor. Since close to the metal-insulator transition temperature the film contains a mixture of metallic and insulating domains, τ_1 and τ_2 can be interpreted as corresponding to domain nucleation and domain growth, respectively. This allows us to calculate a frequency response function f and the phase delay $\Delta\phi$ for the peak-to-peak resistance change under harmonic excitation as

$$\frac{(\Delta R_{\text{strain}}/R_0)_{\text{p-p}}}{(\delta_c)_{\text{p-p}}} = A_0 f(\omega, \tau_1, \tau_2, \alpha), \quad (2)$$

$$\Delta\phi = \Delta\phi(\omega, \tau_1, \tau_2, \alpha), \quad (3)$$

where A_0 (%/%) is a dimensionless strain-resistance conversion ratio and ω is the measurement frequency. Fitting results assuming the double exponential model are shown in Fig. 5(b). A reasonable fit indicates that this is a minimal model for this VO_2 film sample. There are likely additional low-frequency relaxation modes in the system, but these could not be reliably analyzed due to the limited signal-to-noise ratio of the resistance signal. Our main interest is in extracting the most significant time constants, τ_1 and τ_2, which characterize the dynamics of the phase transition, and α, which is a scaling factor describing the ratio between domain nucleation and growth.

The time scales of resistance response to strain change are generally different, depending on whether measurements are done on the insulating or metallic side of the phase transition temperature. The resistance (i.e., temperature, Fig. 2) dependence of the time scale of domain switching can be discussed in terms of τ_1, τ_2, and α. These three parameters can be obtained in two ways, either from the time dependence data, as in Fig. 5(a), or indirectly from the frequency dependence, as in Fig. 5(b). The results of both types of experiments are compared in Fig. 6. It should be noted that the application of stepwise voltage to the piezo actuator deforming the sample does not mean that strain follows a perfect step function for various extrinsic mechanical reasons. Due to that, relaxation time data obtained from the frequency dependence measurements is more reliable. However, the time-domain experiments yielded nearly the same values for the three relaxation model parameters shown in Fig. 6 and thus confirmed that the analysis method is robust and reflects the true intrinsic material properties.

We have interpreted the two time constants in Eq. (1) as corresponding to domain nucleation (fast) and domain growth (slow). This assignment can be understood based on the CT-AFM measurements in Fig. 3. The appearance of new

TABLE I. Areas of domain growth S_{growth} and switching S_{switch} between images (a)–(d) in Fig. 3. Calculated switching ratios, $S_{switch}/(S_{growth}+S_{switch})$ are also shown. These values can be associated with α in Eq. (1).

	(a)⇔(b)	(b)⇔(c)	(c)⇔(d)
$S_{growth}(\mu m^2)$	0.0013	0.0078	0.019
$S_{switch}(\mu m^2)$	0.0034	0.029	0.02
Ratio	0.72	0.79	0.51

metallic domains and the growth of existing domains can be directly determined from the conductivity maps. If the proposed interpretation of the relaxation time constants is valid, the scaling factor α corresponds to the grain switching ratio associated with homogeneous metallic domain nucleation vs growth. The values of α determined from time- and frequency-domain strain measurements are in the range of $\sim 0.7-0.8$ at low temperatures (high resistance), where nucleation dominates and the resistance relaxation lifetime is determined by the probability of switching a single grain in the film. At higher temperatures (low resistance), α drops to ~ 0.5, at which point domain growth becomes more important (Fig. 6), possibly due to an increase of τ_1 in the metallic phase. The data obtained from dynamic strain measurements are similar to the numbers derived from the CT-AFM mappings (Table I). This shows that the assumption that τ_1 and τ_2 correspond to domain nucleation and domain growth is indeed reasonable.

From Fig. 6, it can be seen that the time constant of domain growth, τ_2, remains at around 2–3 ms over the whole measurement temperature range. This indicates that domain growth is mainly affected by thermal energy, $k_B T$, which is essentially constant within the data set, since measurements only have a meaning within a few degrees of the transition temperature. On the other hand, the time constant of domain nucleation, τ_1, is increasing with measurement temperature. It follows that the system is nucleation limited at lower temperature, and both nucleation and growth contribute nearly equally at higher temperature. The reason why τ_1 increases sharply over a narrow sample resistance range can be seen by considering that domain nucleation is mainly affected by the energy barrier between metallic and insulating phases. Below T_c, any grains that switch to metallic state due to the applied strain will rapidly return to the insulating state, giving a fast τ_1 response. The data in Fig. 6 indicates that the height of the energy barrier separating metallic and insulating states is larger at higher temperature, resulting in a metastable system and a slower nucleation lifetime. This result is supported by Vikhnin *et al.*,[16] who calculated the height of the energy barrier in VO_2 as shown in the Fig. 2 inset. They calculated the barrier height with respect to a charge-transfer order parameter q for the tetragonal symmetry, and concluded that the energy barrier is higher for larger q, which corresponds to higher temperature.

IV. CONCLUSIONS

A phase transition induced by dynamic strain in a VO_2 thin film was studied by using a low-frequency crystal bending stage. The frequency response of the thin-film sample to harmonic strain excitation was used to derive two time constants, corresponding to a domain nucleation process ($\tau_1 \sim 10^{-5}$ s) and a domain growth process ($\tau_2 \sim 10^{-3}$ s). It was found that the domain nucleation lifetime, τ_1, increased with temperature due to an increase in the energy barrier height separating the metallic and insulating phases above the transition temperature. The rate of domain growth, determined by τ_2, did not change within the measurement temperature range and was mainly given by thermal energy. The temperature dependence of the domain nucleation vs growth scaling factor α showed that the system was nucleation limited at lower temperature, i.e., when metallic domains started to form in an insulating crystal. At higher temperature, the role of domain growth increased as the conductivity change was strongly affected by the variation of the width of the metallic conduction path. Metallic domain growth in VO_2 thin films appears to be restricted by grain boundaries, resulting in a rather slow response time constant in the millisecond range while the response time of a homogeneous crystal or grain is known to be a much faster, picosecond scale process.[2]

Successful application of strain to an oxide crystal by substrate bending shows that this technique may be useful for the study of various other materials as well, where coexistence of competing phases occurs, such as manganites.[26,27] Compared to other high-frequency strain techniques, such as the use of piezoelectric substrates,[28] the in-plane strain in the crystal bending stage is uniaxial and it is, at least, in principle, possible to study materials that either have anisotropic in-plane transport properties or an anisotropic response to applied strain. The bending technique works independent of substrate material and almost any typical thin-film sample can be studied. Measuring strain response gives access to an additional independent axis in the available variable space, in addition to the usual temperature and carrier density parameters.

ACKNOWLEDGMENTS

We thank Z. Hiroi and Y. Okamoto for providing the V_2O_3 target. We would like to express our gratitude to Y. Hasegawa, T. Eguchi, M. Hamada, and H. Takagi for supporting the CT-AFM measurements. This work was supported by NEDO under Project No. 07E51002a.

*mlippmaa@issp.u-tokyo.ac.jp

[1] F. J. Morin, Phys. Rev. Lett. **3**, 34 (1959).
[2] V. Eyert, Ann. Phys. **11**, 650 (2002).
[3] M. Gurvitch, S. Luryi, A. Polyakov, and A. Shabalov, J. Appl. Phys. **106**, 104504 (2009).
[4] J. B. Goodenough, J. Solid State Chem. **3**, 490 (1971).
[5] K. Okazaki, S. Sugai, Y. Muraoka, and Z. Hiroi, Phys. Rev. B **73**, 165116 (2006).
[6] M. Nakajima, N. Takubo, Z. hiroi, Y. Ueda, and T. Suemoto, J. Lumin. **129**, 1802 (2009).
[7] C. Kübler, H. Ehrke, R. Huber, R. Lopez, A. Halabica, R. F. Haglund, Jr., and A. Leitenstorfer, Phys. Rev. Lett. **99**, 116401 (2007).
[8] P. Baum, D.-S. Yang, and A. H. Zewail, Science **318**, 788 (2007).
[9] G. Gopalakrishnan, D. Ruzmetov, and S. Ramanathan, J. Mater. Sci. **44**, 5345 (2009).
[10] G. Stefanovich, A. Pergament, and D. Stefanovich, J. Phys.: Condens. Matter **12**, 8837 (2000).
[11] T. Kikuzuki and M. Lippmaa, Appl. Phys. Lett. **96**, 132107 (2010).
[12] M. D. Biegalski, K. Dörr, D. H. Kim, and H. M. Christen, Appl. Phys. Lett. **96**, 151905 (2010).
[13] P. A. Bakut, V. E. Kirakosyants, V. A. Loginov, C. J. Solomon, and J. C. Dainty, Opt. Commun. **109**, 10 (1994).
[14] K. Nagashima, T. Yanagida, H. Tanaka, and T. Kawai, Phys. Rev. B **74**, 172106 (2006).
[15] Y. Muraoka, Y. Ueda, and Z. Hiroi, J. Phys. Chem. Solids **63**, 965 (2002).
[16] V. S. Vikhnin, S. Lysenko, A. Rua, F. Fernandez, and H. Liu, Opt. Mater. **29**, 1385 (2007).
[17] H. S. Choi, J. S. Ahn, J. H. Jung, T. W. Noh, and D. H. Kim, Phys. Rev. B **54**, 4621 (1996).
[18] J. Cao, E. Ertekin, V. Srinivasan, W. Fan, S. Huang, H. Zheng, J. W. L. Yim, D. R. Khanal, D. F. Ogletree, J. C. Grossman, and J. Wu, Nat. Nanotechnol. **4**, 732 (2009).
[19] A. P. Klein, J. Phys. C **3**, L66 (1970).
[20] P. U. Jepsen, B. M. Fischer, A. Thoman, H. Helm, J. Y. Suh, R. Lopez, and R. F. Haglund, Jr., Phys. Rev. B **74**, 205103 (2006).
[21] M. M. Qazilbash, M. Brehm, B.-G. Chae, P.-C. Ho, G. O. Andreev, B.-J. Kim, S. J. Yun, A. V. Balatsky, M. B. Maple, F. Keilmann, H.-T. Kim, and D. N. Basov, Science **318**, 1750 (2007).
[22] A. Frenzel, M. M. Qazilbash, M. Brehm, B.-G. Chae, B.-J. Kim, H.-T. Kim, A. V. Balatsky, F. Keilmann, and D. N. Basov, Phys. Rev. B **80**, 115115 (2009).
[23] J. Nag and R. F. Haglund, Jr., J. Phys.: Condens. Matter **20**, 264016 (2008).
[24] Y. J. Chang, C. H. Koo, J. S. Yang, Y. S. Kim, D. H. Kim, J. S. Lee, T. W. Noh, H.-T. Kim, and B. G. Chae, Thin Solid Films **486**, 46 (2005).
[25] S. Lysenko, V. Vikhnin, F. Fernandez, A. Rua, and H. Liu, Phys. Rev. B **75**, 075109 (2007).
[26] J. Hejtmánek, Z. Jirák, J. Šebek, A. Strejc, and M. Hervieu, J. Appl. Phys. **89**, 7413 (2001).
[27] J. F. Mitchell, D. N. Argyriou, A. Berger, K. E. Gray, R. Osborn, and U. Welp, J. Phys. Chem. B **105**, 10731 (2001).
[28] M. C. Dekker, A. D. Rata, K. Boldyreva, S. Oswald, L. Schultz, and K. Dörr, Phys. Rev. B **80**, 144402 (2009).